Research Square

Preprints are preliminary reports that have not undergone peer review.
They should not be considered conclusive, used to inform clinical practice,
or referenced by the media as validated information.

Characterization and considerations of mouse Cre lines targeting cerebellar granule cells in early postnatal development

Rajaram Kshetri
Southern Illinois University – School of Medicine
Matthew Woodbury
Southern Illinois University – School of Medicine
Raheem FH Al Aameri
Southern Illinois University – School of Medicine
Roseline Ewa
Southern Illinois University – School of Medicine
Brandon C Cox
Southern Illinois University – School of Medicine
Ben D Richardson
brichardson29@siumed.edu
Southern Illinois University – School of Medicine

Research Article

Keywords: Cerebellar granule cells, Cerebellum, Cre, Mouse model, Conditional knockout, Shank3

Posted Date: November 13th, 2026

DOI: https://doi.org/10.21203/rs.3.rs-11568385/v1

License: This work is licensed under a Creative Commons Attribution 4.0 International License.
Read Full License

Additional Declarations: No competing interests reported.

Characterization and considerations of mouse Cre lines targeting cerebellar granule cells in early postnatal development

Abbreviated Title: Cerebellar granule cell Cre lines

Authors: Rajaram Kshetri[1], Matthew Woodbury[1], Raheem F H Al Aameri[1], Roseline Ewa[1], Brandon C Cox[1], Ben D Richardson[1]

Affiliations: [1]Department of Pharmacology, Southern Illinois University – School of Medicine, Springfield, IL, United States 62702

Corresponding Author: Ben D Richardson, PhD: brichardson29@siumed.edu

Abstract

The Cre-lox tool is invaluable for cell type-specific genetic manipulation to understand the function of the gene of interest in specific cell types. This study characterizes three Cre-driver lines targeting cerebellar granule cells (CGCs) to then generate an optimal CGC *Shank3* conditional knockout (cKO) mouse. First, we compared the Cre-recombination efficiency of three Cre mouse models for targeting CGCs. We then used the predicted optimal Cre line to delete the *Shank3* gene in CGCs in mice given its expression in CGCs and association with Phelan McDermid Syndrome (PMS) and autism spectrum disorder (ASD). The specificity of Cre recombinase in CGCs was evaluated by using *Atoh1-CreER*^{TM}, *Atoh1-Cre*, and *Nse-CreER*^{T2} lines with *Ai14* reporter mice. *Atoh1-CreER*^{TM} showed the highest specificity and uniform reporter expression across all cerebellar lobes. Therefore, *Atoh1-CreER*^{TM} mice were crossed with *Shank3*$^{fl/fl}$ mice to generate inducible CGC-specific *Shank3* cKO mice that were injected with tamoxifen. To confirm the deletion, *Shank3* mRNA levels in the cerebellum were quantified. Unexpectedly, only a mild reduction of *Shank3* mRNA levels was observed in the cerebellum, which was in contrast with tdTomato expression. These findings highlight the importance of validating functional gene deletion at the mRNA or protein level, independent of reporter fluorescence, when characterizing cKO models. Future studies should explore alternative Cre lines or optimize Cre induction protocols to better understand the cerebellar-specific role of *Shank3*.

Key Words

Cerebellar granule cells, Cerebellum, Cre, Mouse model, Conditional knockout, *Shank3*

Introduction

Conditional gene deletion strategies have transformed neuroscience research by enabling investigators to manipulate gene expression in specific cell populations at defined developmental timepoints (Tsien, 2016; Kim et al., 2018). This became possible with the development of the Cre-lox system in mice, which provided spatiotemporal control over gene deletion (Sauer and Henderson, 1988; Orban et al., 1992; Gu et al., 1994; Tsien et al., 1996). This system uses a driver line that expresses Cre recombinase under the control of a cell-type-specific promoter to excise loxP-flanked ("floxed") genomic segments in a mouse line carrying a "floxed" allele of the gene of interest (Feil et al., 1997; Cox et al., 2012). By restricting genetic ablation to specific neuronal populations or developmental windows, it is possible to dissect the contributions of distinct circuit elements to complex behaviors and disease states (Gavériaux-Ruff and Kieffer, 2007).

A crucial step in conditional gene deletion experiments is verifying that the target locus is correctly recombined in the specific cells at the right time and to a sufficient level to impact gene expression (Schmidt-Supprian and Rajewsky, 2007; Heffner et al., 2012; Becher et al., 2018; Erhardt et al., 2025). Recombinase activity is usually inferred by crossing a driver line with a Cre-dependent reporter allele (such as a *ROSA26* "lox-stop-lox" fluorescent reporter or lacZ), because reporter expression gives a convenient readout of where Cre has been active (Soriano, 1999; Madisen et al., 2009). However, reporter activation does not necessarily mean that the target gene has been excised or inverted. Recombination efficiency can vary with factors such as chromatin accessibility (Long and Rossi, 2009), local sequence context, and the distance between loxP sites (Liu et al., 2013; Luo et al., 2020). As a result, a highly sensitive reporter might indicate widespread recombination even when recombination at a separate floxed allele is partial or mosaic (Madisen et al., 2009; Luo et al., 2020). This issue can be amplified for inducible CreER systems, where recombinase nuclear translocation is temporally constrained by tamoxifen exposure and metabolism (Feil et al., 1997, 2009), and where low-level or transient Cre activity may be sufficient for reporter recombination but insufficient for robust excision of a larger or less permissive target locus (Álvarez-Aznar et al., 2020; Jahncke and Wright,

2024). For these reasons, careful validation of conditional models ideally requires direct measurement of target gene loss (mRNA and/or protein) in addition to reporter-based mapping of Cre activity (Becher et al., 2018; Jahncke and Wright, 2024).

Cerebellar granule cells (CGCs) form the primary input layer of the cerebellar cortex that receives sensorimotor input from mossy fibers (Sassoè-Pognetto and Patrizi, 2013; Rossi and Richardson, 2018). Accumulating evidence implicates cerebellar dysfunction in autism spectrum disorder (ASD), and several ASD-associated genes are expressed in CGCs, including *Shank3* (Soda et al., 2019; Achilly et al., 2021; Kawamura et al., 2021; Kshetri et al., 2024, 2025). Therefore, targeted manipulation of ASD-related genes and other genes that cause ataxia and motor dysfunction in CGCs enables researchers to dissect the specific contributions of this cell type to cerebellar dysfunction and associated CGC-relevant behavioral phenotypes.

To target CGCs, several Cre driver lines have been established using promoters or enhancers active in these neurons or their precursors. The *Atoh1* (*Math1*) promoter, a proneural transcription factor, is expressed in rhombic lip progenitors that give rise to CGCs and unipolar brush cells (Consalez et al., 2013) during embryogenesis. *Atoh1*-driven Cre or an inducible variant (*Atoh1-CreER*^{TM}) target ATOH1-positive precursors, making them valuable for studying gene function during early postnatal cerebellar development when CGC precursors are proliferating and migrating (Chow et al., 2006). Another inducible line, *Nse-CreER*^{T2}, driven by the neuron-specific enolase (*Nse*) promoter, allows for tamoxifen-inducible recombination in CGCs across all cerebellar lobules, including postmitotic CGC-precursors (Pohlkamp et al., 2014). While these tools provide genetic access to CGCs at different developmental stages, systematic comparisons of their specificity and recombination efficiency are lacking.

In this study, we characterize and compare the specificity and efficiency of Cre-mediated recombination in three mouse lines and their established induction protocols (*Atoh1-CreER*^{TM}*, Atoh1-Cre, and Nse-CreER*^{T2}) suitable for targeting CGCs immediately after birth using the *Ai14* tdTomato reporter. We then leverage the most promising line to generate a CGC-specific conditional knockout of

Shank3, a scaffolding protein strongly implicated in ASD (Bozdagi et al., 2010; Drapeau et al., 2018). Our results reveal an important discrepancy between reporter expression and target gene deletion efficiency, underscoring the need to validate conditional knockouts beyond reporter visualization.

Materials & Methods

Animals

All animal experiments were performed in accordance with the protocols approved by the Institutional Animal Care and Use Committee (IACUC). Animal genotypes were determined by Transnetyx (Cordova, TN) using ear punch biopsies. All the experiments were performed in 5-6 weeks old mice.

***Atoh1-CreER^{TM};Ai14* mice:** *Atoh1-CreER^{TM} (Math1-CreER^{TM})* mouse strain (strain: FVB-Tg(Atoh1-cre/ERT)1Sbk/Mmnc, RRID:MMRRC_029581-UNC), originally generated by Dr. Suzanne Baker's laboratory at St. Jude Children's Research Hospital (Memphis, TN) (Chow et al., 2006), were used to generate *Atoh1-CreER^{TM};Ai14* mice by crossing *Atoh1-CreER^{TM}* males, maintained at a C57BL/6J genetic background, with *Ai14* Cre-reporter females (JAX Strain #007914). The generated offspring were injected with tamoxifen (3 mg/40 g body weight; sunflower oil) intraperitoneally (I.P.) at P0 and P1 to activate CreER. CreER^{+} offspring with the tdTomato allele show tdTomato fluorescence in CreER^{+} cells due to Cre-mediated recombination after tamoxifen injection. CreER^{-} offspring with the tdTomato allele were used as controls.

***Atoh1-Cre;Ai14* mice:** *Atoh1-Cre* male mice (maintained on a C57BL/6 background, JAX strain #011104; (Matei et al., 2005)) were acquired from the Jackson Laboratory and then crossed with *Ai14* females to generate *Atoh1-Cre^{+};Ai14^{+}*, and *Atoh1-Cre^{-};Ai14^{+}* (control) offspring. *Atoh1-Cre* constitutively expresses Cre in specific cell types. Subsequently, the specificity of Cre-recombination was assessed by the expression of tdTomato in sagittal brain sections in *Atoh1-Cre^{+};Ai14^{+}* and control mice.

***Nse-CreER^{T2};Ai14* mice:** Another tamoxifen-inducible Cre-line, *Nse-CreER^{T2+},* reported to specifically target CGCs, was obtained from the Jackson Laboratory (maintained on a C57BL/6J background, JAX strain #022763; (Pohlkamp et al., 2014)). Subsequently, *Nse-CreER^{T2+}* mice were crossed with *Ai14*

mice to generate *Nse-CreER^{T2+};Ai14^{+}* and *Nse-CreER^{T2-};Ai14^{+}* (control). Thus, the resultant pups were injected with 150 µg/day of tamoxifen at P1 and P2 (total 300 µg of tamoxifen). ***Atoh1-CreER^{TM};Shank3$^{fl/fl}$* mice (CGC-*Shank3*cKO):** Male *Atoh1-CreER^{TM}* mice were bred in-house with homozygous *Shank3$^{flox\ ex4-22}$* (i.e., *Shank3$^{fl/fl}$*) females (JAX strain #032158) to generate *Atoh1-CreER^{TM};Shank3$^{fl/fl}$* offspring. The *Shank3$^{flox\ ex4-22}$* mice have loxP sites flanking exons 4-22 of the *Shank3* gene, allowing for conditional deletion of *Shank3* in CGCs upon CreER activation after tamoxifen injection (3 mg/40 g, I.P.; sunflower oil) at P0 and P1 in *Atoh1-CreER^{TM+};Shank3$^{fl/fl}$* progeny. The offspring with *Atoh1-CreER^{TM-};Shank3$^{fl/fl}$* genotype were also injected with tamoxifen and used as controls. The efficiency of *Shank3* deletion was assessed by comparing *Shank3* mRNA levels in cerebellar slices between WT and KO using *in situ* hybridization (ISH).

Immunofluorescence

For brain extraction, mice were anesthetized using isoflurane (3-5%) and then transcardially perfused with 1X phosphate-buffered saline (PBS), followed by 4% formaldehyde diluted in 1X PBS. After perfusion, the brains were post-fixed for 24 h in 4% formaldehyde, then placed in sucrose solution gradients until they dropped to the bottom. Sagittal whole-brain slices (30 µm thick) with cerebellar vermis were prepared on a cryostat (Leica CM 1850) at -25 °C. Subsequently, free-floating immunofluorescence staining was performed.

The brain slices were initially placed in 0.01M sodium citrate buffer (pH 6.0), and antigen retrieval was performed at 75 °C for 30 min. The brain slices were then permeabilized in 0.25% Triton X-100 in PBS for 30 min, followed by blocking in IHC/ICC Blocking Buffer (eBiosciences) containing 0.25% Triton X-100 for 1 h. Subsequently, the slices were incubated in primary antibody rabbit IgG anti-NeuN (1:1000, Novus Biologicals, catalog #NBP1-92716) overnight at 4 °C. Slices were then washed with PBS and incubated in secondary antibody donkey IgG anti-rabbit DyLight 488 (1:1000; Thermo Fisher Scientific, catalog #SA5-10038). The nuclei were counterstained with Hoechst 33342 (1:2000, Thermo Fisher Scientific, catalog #H3570). Finally, tissue sections were washed and transferred to glass slides and mounted with Prolong Gold (Invitrogen). Imaging of NeuN-positive CGCs in the

granule cell layer of the cerebellum from the stained brain slices was performed by capturing Z-stack images containing 3 optical slices at an interval of 1 μm using a 40X oil immersion objective (NA 1.3) on a confocal microscopy system (Zeiss LSM800) at a resolution of 1024 × 1024 pixels. Image acquisition settings were held constant across samples within each quantitative experiment.

Cre-line validation by tdTomato reporter expression: To assess Cre recombination efficiency, the percentage of NeuN-positive CGCs expressing tdTomato was quantified manually within a 50 × 50 μm² region of interest placed in the granule cell layer across cerebellar lobules 2-10 using ZEN Lite software (v3.7; Zeiss). Two sections per animal were analyzed, and data were averaged per mouse (N = 3 mice per Cre line).

After manual analysis, Cre recombination efficiency was also quantified using an in-house automated Fiji/ImageJ pipeline. Confocal Z-stacks were imported using the Bio-Formats plugin (Linkert et al., 2010), and the optical slice with the highest mean NeuN intensity was selected (with optional manual Z selection when needed). Each channel underwent thresholding and despeckling steps to reduce noise prior to mask generation, and all masks underwent a morphological opening operation prior to analysis to improve noise reduction and smoothing. For each channel (tdTomato, NeuN, Hoechst), the Trainable Weka Segmentation package was utilized to train a model using the Fast Random Forest classifier (source code: https://github.com/MKWoodbury/SegmentAndCalculate.git), with the trained models then used to generate binary masks for each channel (Breiman, 2001; Arganda-Carreras et al., 2017). The granule cell region of interest was defined as the colocalized area for both NeuN and Hoechst-positive pixels, and tdTomato-positive granule-cell signal as pixels positive for all three channels (i.e, tdTomato, NeuN, and Hoechst). Recombination efficiency was calculated as (tdTomato + NeuN + Hoechst colocalized pixels)/(NeuN + Hoechst colocalized pixels) × 100%. Automated results closely matched manual quantification in *Atoh1-CreER^{TM+};Ai14^{+}* mice (Fig. 1J); therefore, automated analysis was used to quantify reporter expression efficiency in *Atoh1-Cre^{+};Ai14^{+}* and *Nse-CreER^{T2+};Ai14^{+}* mice. We note that this automated analysis reflects a pixel-based quantification and not the number of colocalized soma. However, the pixel-based analysis was in

agreement with manual analyses of cell bodies positive for each marker and accurately reflects the proportion of cells for each classification (Fig. 1J). While this may not be appropriate for all cell types or all stains, we do find this particular approach works well when in the cerebellar granule cell layer, where neurons of interest are relatively homogeneous in size and shape. Image analyses were performed with the investigator blinded to genotype and experimental group; sample identities were decoded only after completion of the analysis.

***In situ* hybridization (ISH)**

This efficiency of Cre activity was further confirmed by quantifying *Shank3* mRNA expression in *Atoh1-CreER^{TM};Shank3$^{fl/fl}$* mice using an *in situ* hybridization assay. *In situ* hybridization was performed using the RNAscope™ Multiplex Fluorescent Reagent Kit v2 (Advanced Cell Diagnostics, Newark, CA) according to the manufacturer's protocol. First, the brain slices (30 µm thickness) were dehydrated by immersing the slides in a series of ethanol solutions of increasing concentration (50%, 70%, and 100%) for 5 minutes each at room temperature. Next, the brain slices were treated with RNAscope Hydrogen Peroxide for 10 min, then antigen-retrieved with RNAscope 1X target retrieval reagent at 100 °C for 15 min. The slices were then treated with RNAscope Protease III and incubated in a hybridization oven at 40 °C for 30 min. We used the RNAscope probe for mouse *Shank3* mRNA (ACD, catalog #417371), which detects the *Shank3* mRNA transcript exons 11-20, specifically targeting base pairs 1488-2346. The slides were incubated in a hybridization oven at 40 °C for 2 h after the target probe was added. Following probe hybridization, the slides were washed with washing buffer and incubated with signal amplification reagents in the hybridization oven at 40 °C for 15 min. Finally, the slides were washed and mounted with Prolong Gold (Invitrogen). Airyscan imaging of the cerebellar lobes was performed by capturing Z-stack images containing 6 optical slices at an interval of 1 µm using a 10X objective (NA 0.3) on a confocal microscopy system (Zeiss LSM800) at a resolution of 1000 × 1000 pixels.

Data analysis: Each Z-stack image was processed to create a single orthogonal projection image using ZEN Lite software (version 3.7; Zeiss). The fluorescence intensity of the *Shank3* transcript was then measured in a 100 × 100 µm² area in the granule cell layer. To quantify background intensity, a 10 × 10

μm^2 square box was placed in the white matter fiber region, where *Shank3* is not expressed. The background intensity was subtracted from the previously measured *Shank3* transcript fluorescence intensity to obtain the actual fluorescence intensity in the image. Finally, the Shank3 mRNA intensity was normalized to the mean GC intensity value from wildtype mouse tissue sections, which was included as a positive control on each slide. Two images from each animal were analyzed, with three animals per genotype.

Results

Atoh1-CreER^{TM} drives robust and cerebellum-specific tdTomato expression.

Atoh1-CreER^{TM+};Ai14^{+} offspring (Fig. 1A) showed robust tdTomato fluorescence restricted to the cerebellum, with no detectable nonspecific expression in other brain regions (Fig. 1B). The Cre-negative offspring with the tdTomato allele were used as a control, which did not show tdTomato expression (Fig. 1F), confirming that the reporter expression was Cre-dependent. To quantify reporter labeling efficiency, we compared manual counting of tdTomato^{+} CGCs with an automated image-analysis approach that quantified the colocalized tdTomato and NeuN surface area across 33 high-magnification (40X) images collected from cerebellar lobules 2-10 in four *Atoh1-CreER^{TM+};Ai14^{+}* mice (one sagittal section per mouse). Both approaches produced comparable results (Fig. 1J), supporting the reliability of the automated quantification, which was used in subsequent analyses in *Atoh1-Cre^{+};Ai14^{+}* (Fig. 2J, K) and *Nse-CreER^{T2+};Ai14^{+}* mice (Fig. 3J, K). The reporter signal was uniformly distributed across cerebellar lobes, with each lobe showing at least 80% of tdTomato-positive CGCs (Fig. 1K). This CreER-line showed a very specific and robust expression of tdTomato in the majority of the CGCs (Fig. 1L), suggesting that the *Atoh1-CreER^{TM}*-mediated recombination could achieve high specificity and efficiency in manipulating loxP-flanked gene expression in CGCs (i.e. deleting *Shank3* when crossed with *Shank3$^{fl/fl}$* mice).

Atoh1-Cre line exhibits ectopic and variable tdTomato expression within the cerebellum.

Cre-positive *Atoh1-Cre;Ai14* mice (Fig. 2A) carrying the tdTomato allele (*Atoh1-Cre^{+};Ai14^{+})* showed tdTomato expression in the cerebellum, along with some ectopic expression observed in other

brain regions, including the superior colliculus, CA2 region of the hippocampus, hypothalamus, and pons (Fig. 2B). Cre-negative *Ai14* littermate controls did not show tdTomato expression (Fig. 2F), confirming that Cre-recombination induces the reporter expression. Additionally, within the cerebellum, tdTomato labeling varied across lobules, with lobe 10 showing the lowest expression (Fig. 2B, J). Compared with *Atoh1-CreER^{TM+};Ai14^{+}* mice, the *Atoh1-Cre* line results suggest lower specificity and lower efficiency in lobe 10 for targeting CGCs (Fig. 2J). However, when pooled across cerebellar lobules, overall tdTomato labeling in CGCs was comparable between *Atoh1-CreER^{TM+};Ai14^{+}* and *Atoh1-Cre^{+};Ai14^{+}* lines *(*Fig. 2K).

Nse-CreER^{T2} line exhibits low and ectopic tdTomato expression

We tested another, but less often used, tamoxifen-inducible Cre-line (*Nse-CreER^{T2};Ai14*) generated by crossing *Nse-CreER^{T2}* with *Ai14* (tdTomato reporter) mice (Fig. 3A). Cre-positive offspring carrying the tdTomato allele (*Nse-CreER^{T2+};Ai14^{+})* showed tdTomato expression in the cerebellum, along with ectopic expression in other brain regions, including the superior colliculus, dentate gyrus of the hippocampus, and medial vestibular nuclei (Fig. 3B). Similar to *Atoh1-Cre^{+};Ai14^{+}* mice, *Nse-CreER^{T2+};Ai14^{+}* mice demonstrated off-target reporter expression. Cre-negative *Ai14* littermate controls showed no tdTomato signal (Fig. 3F), confirming that reporter expression is Cre-dependent. Interestingly, the reporter signal appears variable across the cerebellar lobes (Fig. 3J) with a subset of CGCs labeled with tdTomato. Among the three Cre lines tested, the *Nse-CreER^{T2}* line showed the lowest and most variable tdTomato labeling for CGCs (Fig. 3J, K).

Atoh1-Cre and _Nse-CreER^{T2}_ lines show distinct patterns of off-target tdTomato expression in extra-cerebellar regions

To elucidate off-target recombination observed in *Atoh1-Cre^{+};Ai14^{+}* (Fig. 2B) and *Nse-Cre^{+};Ai14^{+}* mice (Fig. 3B), we examined higher-magnification images of tdTomato signal in representative extra-cerebellar regions (Fig. 4A-G). In the *Atoh1-Cre^{+};Ai14^{+}* line, tdTomato fluorescence was detected in the hippocampus (prominently within the CA2 region), hypothalamus, superior colliculus, and pons (Fig. 4A-D). In *Nse-Cre^{+};Ai14^{+}* mice, tdTomato expression was observed

in the hippocampus (dentate gyrus), superior colliculus, and medial vestibular nuclei (Fig. 4E-G). These higher-magnification images confirm that both Cre lines drive tdTomato expression outside the cerebellum. Some off-target regions overlap between lines (e.g., the superior colliculus), whereas others are line-specific. For example, *Atoh1-Cre* labels hippocampal CA2 and hypothalamus, while *Nse-CreER^{T2}* labels the dentate gyrus and medial vestibular nuclei.

All three Cre-lines with tdTomato reporter, i.e., *Atoh1-CreER^{TM+};Ai14^{+}*, *Atoh1-Cre^{+};Ai14^{+}*, and *Nse-CreER^{T2+};Ai14^{+}*, were validated to assess the specific expression of tdTomato in the granule cell layer of the cerebellar cortex. Cre-negative mice with tdTomato reporter-positive alleles, i.e., *Atoh1-CreER^{TM-};Ai14^{-}* (with tamoxifen injection), *Atoh1-Cre^{-};Ai14^{-}*, and *Nse-CreER^{T2-};Ai14^{-}* (with tamoxifen injection), were used as controls. The Cre-line that showed the most specific tdTomato expression in the granule cell layer, with minimal or no off-target expression in other brain regions, was selected for further analysis.

Shank3 mRNAscope signal in the cerebellar granule cell layer following _Atoh1-CreER^{TM}_ induction

After characterizing tdTomato labeling in all three Cre-lines (and associated Cre-induction tamoxifen treatment protocols) that might be considered for targeting postnatal CGCs, we found that the *Atoh1-CreER^{TM}* line showed spatially restricted reporter expression within the cerebellum and the most uniform reporter coverage across cerebellar lobules in the brain sections examined. Based on these findings, we selected the *Atoh1-CreER^{TM}* line to conditionally delete *Shank3* from CGCs which typically express *Shank3* uniformly across cerebellar lobules. To generate CGC-specific *Shank3* cKO mice, *Atoh1-CreER^{TM+}* mice were crossed with *Shank3$^{fl/fl}$*. The resultant pups were injected with tamoxifen at P0 and P1 to induce CreER recombination and excise exons 4-22 of *Shank3* specifically in CGCs (Fig. 5A, B). Next, the efficiency of CreER-loxP-mediated deletion of the *Shank3* gene was evaluated by quantifying *Shank3* mRNA levels within the GC layer of the cerebellum, composed primarily of GCs, using fluorescent *in situ* hybridization, which detects *Shank3* transcript exons 11-20. Unexpectedly, our cKO mice showed only a small (~22%) reduction in *Shank3* mRNA puncta

expression when compared to Cre-negative controls (Fig. 5C-E), despite complete *Shank3* deletion reported in the literature when crossed with *CMV-Cre* mice (Drapeau et al., 2018).

Discussion

In this study, the three Cre mouse lines (*Atoh1-CreER^{TM}*, *Atoh1-Cre*, and *Nse-CreER^{T2}*) and their established widely-used induction protocols showed distinct Ai14 reporter-labeling patterns in cerebellar granule cells and extra-cerebellar brain regions. Based on the reporter expression, we selected *Atoh1-CreER^{TM}*, which showed the most robust, selective, and uniform tdTomato expression across the cerebellar lobules within the granule cell layer. Despite the promising reporter signal, *Shank3* deletion in *Atoh1-CreER^{TM+};Shank3$^{fl/fl}$* mice was limited.

We tested *Atoh1-Cre*, which constitutively expresses Cre and has been used in some previous studies (Pan et al., 2009; Lorenz et al., 2011; Wijayatunge et al., 2018; Achilly et al., 2021; Kawamura et al., 2021; Wang et al., 2021) to target the gene of interest in CGCs. Except for Pan et al., which showed LacZ expression in the cochlear nucleus, other studies have not reported off-target reporter expression in brain regions other than the cerebellum. By using the *Atoh-Cre* line, Katayama et al. and Kawamura et al. both reported a low Cre recombinase activity at the posterior lobes in the cerebellum, which aligns with low tdTomato expression in lobe 10 in *Atoh1-Cre* line in our study (Fig. 2B, J) (Kawamura et al., 2021; Katayama et al., 2022).

The off-target reporter expression observed in *Atoh1-Cre* and *Nse-CreERT^{2}* lines highlights the complexities of using sensitive Cre-loxP systems for cell-type-specific targeting. The ectopic tdTomato signal detected in the *Atoh1-Cre* line (Fig. 4A-D) within the pons and hippocampus likely reflects the developmental lineage history of *Atoh1*-expressing progenitors (Wang et al., 2005; Wu et al., 2023), whereas tdTomato signal in the hypothalamus and superior colliculus may, at least in part, reflect projections of Atoh1-lineage neurons to these regions (Karthik et al., 2022; Zhang et al., 2024). It is well-established that the Atoh1-expressing rhombic lip lineages give rise to multiple glutamatergic populations beyond CGCs, including neurons of the precerebellar pontine nuclei (MacHold and Fishell, 2005; Machold et al., 2011). Furthermore, transient *Atoh1* expression has been previously documented

294 in the hippocampal primordium during embryogenesis (MacHold and Fishell, 2005), in which the *Ai14*
295 reporter permanently marks due to its cumulative lineage-tracing nature. Similarly, sparse dentate-
296 gyrus recombination and reporter-positive fibers in the superior colliculus and medial vestibular nuclei
297 observed in the *Nse-CreER*^{T2} line (Fig. 4E-G) are consistent with the original characterization of this
298 transgenic line (Pohlkamp et al., 2014).
299 Unlike *Atoh1-Cre* and *Nse-CreER*^{T2} lines, the *Atoh1-CreER*^{TM} line showed promising results
300 with highly specific and uniform tdTomato expression in the majority of the CGCs (Fig. 1B, K, and L),
301 which is in line with the previous study that generated this line (Chow et al., 2006). This finding led us to
302 predict that the *Atoh1-CreER*^{TM} line would be effective for the conditional deletion of the *Shank3* gene
303 in the CGC population. To generate a conditional deletion of the *Shank3* gene in CGCs, we crossed
304 *Shank3*$^{fl/fl}$ mice with the *Atoh1-CreER*^{TM} line. Unexpectedly, our cKO mice revealed only a mild
305 reduction in *Shank3* mRNA levels in the cerebellum compared to controls (Fig. 5C-E). This discrepancy
306 between highly efficient reporter gene activation and limited target gene deletion may be attributed to
307 several factors.
308 First, while reporter lines serve as valuable indicators of where and when Cre is expressed and
309 capable of recombination (Madisen et al., 2009; Luo et al., 2020; Jahncke and Wright, 2024), they do
310 not directly report the recombination efficiency of a specific target locus. The efficiency of Cre-mediated
311 recombination is not uniform across all genomic loci, and different floxed alleles exhibit varying
312 sensitivities to Cre-mediated recombination (Zheng et al., 2000; Luo et al., 2020; Jahncke and Wright,
313 2024; Liu et al., 2013). Reporter constructs, like the *Ai14* line are engineered to be easily accessible
314 and are highly responsive to Cre by inserting into the *ROSA26* locus, rely on the CAG promoter, and
315 the woodchuck hepatitis virus post-transcriptional regulatory element (WPRE) to enhance mRNA
316 stability (Madisen et al., 2009, 2015), together leading to efficient recombination even with relatively low
317 or transient Cre activity (Madisen et al., 2009; Liu et al., 2013; Luo et al., 2020; Álvarez-Aznar et al.,
318 2020). The fluorescence of tdTomato is ~2.8 times brighter than eGFP (often requiring immunostaining
319 amplification) and is readily detected compared to eGFP or other reporters (Madisen et al., 2009,

2015).

Therefore, compared to tdTomato reporter characterization data, the efficiency of recombination at a target gene locus can be significantly lower, potentially requiring higher levels or more prolonged expression of Cre (Liu et al., 2013). The duration of *CreER*^{TM} activity following tamoxifen administration is transient, dependent on the metabolism of tamoxifen and the turnover of the fusion protein (Feil et al., 1997). While this transient activity might be sufficient to trigger recombination at a highly sensitive reporter locus, efficient deletion of a gene at a different locus like *Shank3* might need more sustained Cre activity or a higher peak level of Cre expression within the targeted cells.

Second, the distance between the *loxP* sites can also influence the efficiency of Cre-mediated excision. Longer distances between *loxP* sites, or particular sequence motifs, can reduce recombination efficacy (Zheng et al., 2000; Wang et al., 2009; Liu et al., 2013). The *Shank3*$^{fl/fl}$ allele used in this study contains *loxP* sites located after exons 3, 9, and 22 (Fig. 5B). The original study (Drapeau et al., 2018) used *Shank3*$^{fl/fl}$ with a *CMV-Cre* line to produce germline *Shank3* mice used in this study, which resulted in a constitutive deletion of all major *Shank3* isoforms. The *Shank3* gene is relatively large (~58 kb) (Wang et al., 2011, 2014; Kouser et al., 2013) and the *loxP* sites flanking the region targeted for deletion (exons 4-22) span a substantial genomic distance that may hinder Cre-mediated recombination efficiency, potentially contributing to the incomplete or variable Shank3 deletion observed in cKO models. Although the *Atoh1-CreER*^{TM} line did not show high efficiency for deleting a large segment encompassing exons 4-22 of the *Shank3* gene, it may be useful for deleting small exon segments, such as exons 4-9 or exons 13-16, which target only specific *Shank3* isoforms. In addition, this Cre line may be well suited for the conditional deletion of other genes with relatively short floxed intervals in Atoh1-lineage cerebellar granule cell precursors during early postnatal development. For example, conditional deletion of ~1 exon of *Sox2* in the vestibular system with the *Atoh1-CreER*^{TM} was remarkably efficient (Stone et al., 2021).

Another reason for less efficient deletion of the *Shank3* gene by *Atoh1-CreER*^{TM} driver might be mosaic deletion within the target cell population or incomplete deletion within individual cells (e.g.,

deletion of only one of the two floxed alleles) (Jahncke and Wright, 2024). While the reporter signal may appear widespread, indicating potential recombination, the complete *Shank3* deletion across the entire CGC population could be considerably lower because some cells may have a heterozygous Shank3 deletion, resulting in a modest overall reduction in the mRNA signal. Comparing reporter expression with target protein loss in other Cre lines has highlighted such discrepancies, where the reporter signal does not always predict complete loss of the target protein (Luo et al., 2020; Jahncke and Wright, 2024).

This study has some limitations. First, since the Cre lines were examined using unique driver configurations and established induction regimens, the results characterize reporter labeling under the specific conditions tested rather than the intrinsic recombination efficiencies of the three lines. Second, the extra-cerebellar labeling was assessed in selected sagittal sections and should therefore be interpreted as a qualitative description of the observed reporter distribution rather than a comprehensive brain-wide analysis. In addition, the automated analysis quantified the tdTomato-positive fraction of a NeuN- and Hoechst-defined granule-cell-layer mask and therefore represents a pixel-based measure of reporter coverage rather than a direct count of recombined cells. Finally, the *Shank3* RNAscope analysis measured background-corrected regional fluorescence from a probe targeting exons 11–20 and did not directly assess genomic recombination, transcript abundance in individually identified reporter-positive cells, or SHANK3 protein. Consequently, the observed difference between robust Ai14 labeling and the more modest reduction in *Shank3* RNAscope signal demonstrates that reporter activation did not correspond to a comparable change in the measured *Shank3* transcript signal under these experimental conditions. As such, this key discrepancy underscores the importance of establishing true recombination efficacy for target genes as opposed to using reporter lines (e.g., tdTomato) as a proxy. Dramatic differences, like those identified here, may be essential in interpreting cellular or behavioral functional data in comparable approaches.

To address these limitations and achieve efficient conditional deletion of *Shank3* in CGCs, future studies could consider alternative approaches. These could include testing alternative Cre driver

lines targeting CGCs, such as the constitutive GABAA receptor α6 subunit-Cre line (*Gabra6-Cre*), which may yield better results (Aller et al., 2003; Maejima et al., 2013; Rudolph et al., 2020; Lee et al., 2023). *Gabra6* is selectively expressed in CGCs and a subset of pre-cerebellar nuclei, and has been used to drive Cre expression in CGCs (Aller et al., 2003; Maejima et al., 2013). Since this line is reported to initiate recombination relatively late in postnatal development, peaking around P14, *Gabra6-Cre* is limited to asynchronously targeting mature CGCs (Aller et al., 2003; Choi et al., 2021). Additionally, the *Grin2C-Cre* line is another Cre line for targeting mature CGCs. The promoter of the *Grin2c* gene, which encodes the GluN2C subunit of the NMDA receptor, is active in mature CGCs (Otsuka et al., 2016). Alternatively, optimizing the tamoxifen induction protocol by empirically testing different doses, frequencies, or timings of tamoxifen delivery in the *Atoh1-CreER^{TM}* line might improve the efficiency of deleting exons 4-22 of the *Shank3* gene (Cox et al., 2012; McGovern et al., 2017).

Conclusion

This study compared multiple Cre lines to identify the most efficient line for conditionally deleting genes of interest in CGCs. Comparing three Cre-driver lines, we identified that the *Atoh1-CreER^{TM}* line exhibits specific, uniform, and robust reporter gene expression compared with *Atoh1-Cre* and *Nse-CreER^{T2}* lines. Even with high reporter expression, we observed only a mild reduction in *Shank3* mRNA in the cerebellar granule cell layer. These results highlight the importance of ensuring mRNA or protein expression levels, in addition to mapping potential Cre activity using reporter alleles, when characterizing a cKO mouse model. Future studies should explore alternative Cre drivers that yield high recombination efficiency for manipulating *Shank3* or similar length regions in the CGCs.

Author Contributions: RK, BCC, and BDR designed research; RK, MW, RFHA, and RE performed research; RK and MW analyzed data; BDR oversaw data collection and analysis; RK drafted the paper, which was edited by BDR, MW, and BCC.

Acknowledgments: None

Conflicts of Interest: Authors report no conflicts of interest.

Funding Sources: R01MH129749 to BDR

References

Achilly NP, He LJ, Kim OA, Ohmae S, Wojaczynski GJ, Lin T, Sillitoe RV, Medina JF, Zoghbi HY (2021) Deleting mecp2 from the cerebellum rather than its neuronal subtypes causes a delay in motor learning in mice. eLife 10:e64833.

Aller MI, Jones A, Merlo D, Paterlini M, Meyer AH, Amtmann U, Brickley S, Jolin HE, McKenzie ANJ, Monyer H, Farrant M, Wisden W (2003) Cerebellar granule cell Cre recombinase expression. Genesis 36:97–103.

Álvarez-Aznar A, Martínez-Corral I, Daubel N, Betsholtz C, Mäkinen T, Gaengel K (2020) Tamoxifen-independent recombination of reporter genes limits lineage tracing and mosaic analysis using CreERT2 lines. Transgenic Res 29:53–68.

Arganda-Carreras I, Kaynig V, Rueden C, Eliceiri KW, Schindelin J, Cardona A, Sebastian Seung H (2017) Trainable Weka Segmentation: a machine learning tool for microscopy pixel classification. Bioinformatics 33:2424–2426.

Becher B, Waisman A, Lu L-F (2018) Conditional Gene-Targeting in Mice: Problems and Solutions. Immunity 48:835–836.

Bozdagi O, Sakurai T, Papapetrou D, Wang X, Dickstein DL, Takahashi N, Kajiwara Y, Yang M, Katz AM, Scattoni M, Harris MJ, Saxena R, Silverman JL, Crawley JN, Zhou Q, Hof PR, Buxbaum JD (2010) Haploinsufficiency of the autism-associated Shank3 gene leads to deficits in synaptic function, social interaction, and social communication. Molecular Autism 1:15.

Breiman L (2001) Random Forests. Machine Learning 45:5–32.

Choi JM, Acharya R, Marasini S, Narayan B, Lee KW, Hwang WS, Chang DY, Kim SS, Suh-Kim H (2021) Cell Type-specific Knockout with Gli1-mediated Cre Recombination in the Developing Cerebellum. Experimental Neurobiology 30:203.

Chow LML, Tian Y, Weber T, Corbett M, Zuo J, Baker SJ (2006) Inducible Cre recombinase activity in mouse cerebellar granule cell precursors and inner ear hair cells. Developmental Dynamics 235:2991–2998.

Consalez GG, Florio M, Massimino L, Croci L (2013) Proneural Genes and Cerebellar Neurogenesis in the Ventricular Zone and Upper Rhombic Lip In: Handbook of the Cerebellum and Cerebellar Disorders (Manto M, Schmahmann JD, Rossi F, Gruol DL, Koibuchi N eds), pp23–41. Dordrecht: Springer Netherlands.

Cox BC, Liu Z, Lagarde MMM, Zuo J (2012) Conditional Gene Expression in the Mouse Inner Ear Using Cre-loxP. JARO: Journal of the Association for Research in Otolaryngology 13:295.

Drapeau E, Riad M, Kajiwara Y, Buxbaum JD (2018) Behavioral phenotyping of an improved mouse model of Phelan–McDermid syndrome with a complete deletion of the Shank3 gene. eNeuro 5.

Erhardt V, Hartig E, Lorenzo K, Megathlin HR, Tarchini B, Hosur V (2025) Systematic optimization and prediction of cre recombinase for precise genome editing in mice. Genome Biol 26:85.

Feil R, Wagner J, Metzger D, Chambon P (1997) Regulation of Cre Recombinase Activity by Mutated Estrogen Receptor Ligand-Binding Domains. Biochemical and Biophysical Research Communications 237:752–757.

Feil S, Valtcheva N, Feil R (2009) Inducible Cre mice In: Gene Knockout Protocols , Methods in Molecular Biology.

Gavériaux-Ruff C, Kieffer BL (2007) Conditional gene targeting in the mouse nervous system: Insights into brain function and diseases. Pharmacol Ther 113:619–634.

Gu H, Marth JD, Orban PC, Mossmann H, Rajewsky K (1994) Deletion of a DNA polymerase beta gene segment in T cells using cell type-specific gene targeting. Science 265:103–106.

Heffner CS, Herbert Pratt C, Babiuk RP, Sharma Y, Rockwood SF, Donahue LR, Eppig JT, Murray SA (2012) Supporting conditional mouse mutagenesis with a comprehensive cre characterization resource. Nat Commun 3:1218.

Jahncke JN, Wright KM (2024) Tools for Cre-Mediated Conditional Deletion of Floxed Alleles from Developing Cerebellar Purkinje Cells. eNeuro 11.

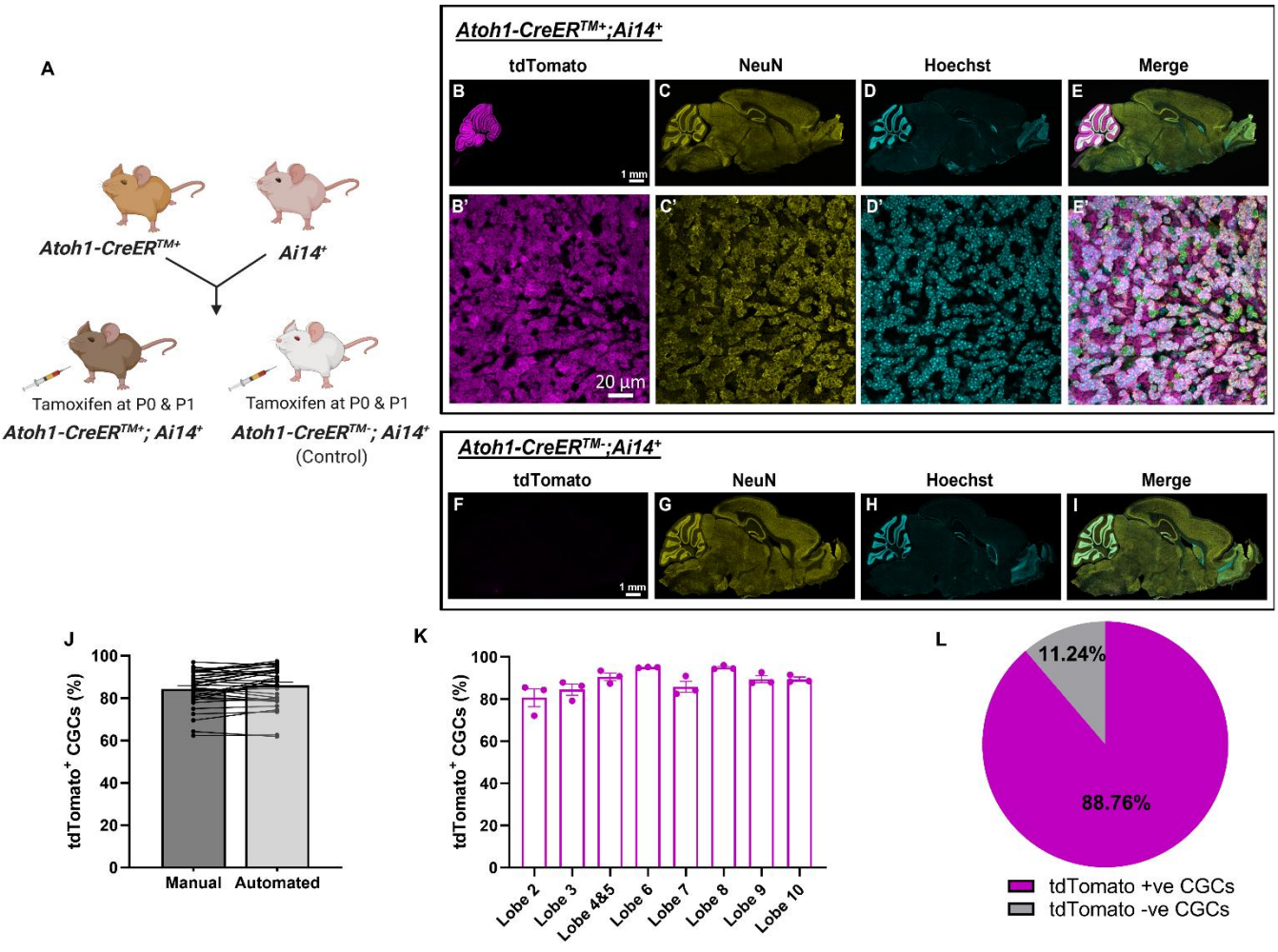
Karthik S, Huang D, Delgado Y, Laing JJ, Peltekian L, Iverson GN, Grady F, Miller RL, McCann CM, Fritzsch B, Iskusnykh IY, Chizhikov VV, Geerling JC (2022) Molecular ontology of the parabrachial nucleus. J Comp Neurol 530:1658–1699.
Katayama K, Zheng Y, Inoue N (2022) Rac-deficient cerebellar granule neurons die before they migrate to the internal granule layer. Sci Rep 12:14848.
Kawamura A, Katayama Y, Kakegawa W, Ino D, Nishiyama M, Yuzaki M, Nakayama KI (2021) The autism-associated protein CHD8 is required for cerebellar development and motor function. Cell Reports 35:108932.
Kim H, Kim M, Im S-K, Fang S (2018) Mouse Cre-LoxP system: general principles to determine tissue-specific roles of target genes. Lab Anim Res 34:147–159.
Kouser M, Speed HE, Dewey CM, Reimers JM, Widman AJ, Gupta N, Liu S, Jaramillo TC, Bangash M, Xiao B, Worley P, Powell C (2013) Loss of Predominant Shank3 Isoforms Results in Hippocampus-Dependent Impairments in Behavior and Synaptic Transmission. The Journal of Neuroscience 33:18448–18468.
Kshetri R, Al Aameri RFH, Richardson BD (2025) Shank3 establishes AMPA receptor subunit composition at cerebellar mossy fiber-granule cell synapses and is associated with altered regional microglial morphology. Neurobiology of Disease 217:107191.
Kshetri R, Beavers JO, Hyde R, Ewa R, Schwertman A, Porcayo S, Richardson BD (2024) Behavioral decline in Shank3Δex4–22 mice during early adulthood parallels cerebellar granule cell glutamatergic synaptic changes. Molecular Autism 15:1–21.
Lee JH, Khan MM, Stark AP, Seo S, Norton A, Yao Z, Chen CH, Regehr WG (2023) Cerebellar granule cell signaling is indispensable for normal motor performance. Cell Reports 42:112429.
Linkert M, Rueden CT, Allan C, Burel J-M, Moore W, Patterson A, Loranger B, Moore J, Neves C, Macdonald D, Tarkowska A, Sticco C, Hill E, Rossner M, Eliceiri KW, Swedlow JR (2010) Metadata matters: access to image data in the real world. J Cell Biol 189:777–782.
Liu J, Willet SG, Bankaitis ED, Xu Y, Wright C, Gu G (2013) Non-parallel recombination limits Cre-LoxP-based reporters as precise indicators of conditional genetic manipulation. Genesis 51:436–442.
Long MA, Rossi FMV (2009) Silencing Inhibits Cre-Mediated Recombination of the Z/AP and Z/EG Reporters in Adult Cells. PLoS One 4:e5435.
Lorenz A, Deutschmann M, Ahlfeld J, Prix C, Koch A, Smits R, Fodde R, Kretzschmar HA, Schüller U (2011) Severe Alterations of Cerebellar Cortical Development after Constitutive Activation of Wnt Signaling in Granule Neuron Precursors ▿ . Mol Cell Biol 31:3326–3338.
Luo Lin et al. (2020) Optimizing Nervous System-Specific Gene Targeting with Cre Driver Lines: Prevalence of Germline Recombination and Influencing Factors. Neuron 106:37-65.e5.
MacHold R, Fishell G (2005) Math1 is expressed in temporally discrete pools of cerebellar rhombic-lip neural progenitors. Neuron 48:17–24.
Machold R, Klein C, Fishell G (2011) Genes expressed in Atoh1 neuronal lineages arising from the r1/isthmus rhombic lip. Gene expression patterns : GEP 11:349.
Madisen L et al. (2015) Transgenic mice for intersectional targeting of neural sensors and effectors with high specificity and performance. Neuron 85:942–958.
Madisen L, Zwingman TA, Sunkin SM, Oh SW, Zariwala HA, Gu H, Ng LL, Palmiter RD, Hawrylycz MJ, Jones AR, Lein ES, Zeng H (2009) A robust and high-throughput Cre reporting and characterization system for the whole mouse brain. Nature Neuroscience 2009 13:1 13:133–140.
Maejima T, Wollenweber P, Teusner LUC, Noebels JL, Herlitze S, Mark MD (2013) Postnatal Loss of P/Q-Type Channels Confined to Rhombic-Lip-Derived Neurons Alters Synaptic Transmission at the Parallel Fiber to Purkinje Cell Synapse and Replicates Genomic Cacna1a Mutation Phenotype of Ataxia and Seizures in Mice. J Neurosci 33:5162–5174.

Matei V, Pauley S, Kaing S, Rowitch D, Beisel KW, Morris K, Feng F, Jones K, Lee J, Fritzsch B (2005) Smaller inner ear sensory epithelia in Neurog1 null mice are related to earlier hair cell cycle exit. Developmental Dynamics 234:633–650.
McGovern MM, Brancheck J, Grant AC, Graves KA, Cox BC (2017) Quantitative Analysis of Supporting Cell Subtype Labeling Among CreER Lines in the Neonatal Mouse Cochlea. JARO 18:227–245.
Orban PC, Chui D, Marth JD (1992) Tissue- and site-specific DNA recombination in transgenic mice. Proc Natl Acad Sci U S A 89:6861–6865.
Otsuka S, Konno K, Abe M, Motohashi J, Kohda K, Sakimura K, Watanabe M, Yuzaki M (2016) Roles of Cbln1 in Non-Motor Functions of Mice. J Neurosci 36:11801–11816.
Pan N, Jahan I, Lee JE, Fritzsch B (2009) Defects in the cerebella of conditional Neurod1 null mice correlate with effective Tg(Atoh1-cre) recombination and granule cell requirements for Neurod1 for differentiation. Cell Tissue Res 337:407–428.
Pohlkamp T, Steller L, May P, Günther T, Schüle R, Frotscher M, Herz J, Bock HH (2014) Generation and Characterization of an Nse-CreERT2 Transgenic Line Suitable for Inducible Gene Manipulation in Cerebellar Granule Cells. PLoS ONE 9:e100384.
Rossi DJ, Richardson BD (2018) The Cerebellar GABAAR System as a Potential Target for Treating Alcohol Use Disorder. Handb Exp Pharmacol 248:113–156.
Rudolph S, Guo C, Pashkovski SL, Osorno T, Gillis WF, Krauss JM, Nyitrai H, Flaquer I, El-Rifai M, Datta SR, Regehr WG (2020) Cerebellum-Specific Deletion of the GABAA Receptor δ Subunit Leads to Sex-Specific Disruption of Behavior. Cell Reports 33:108338.
Sassoè-Pognetto M, Patrizi A (2013) Development of Glutamatergic and GABAergic Synapses In: Handbook of the Cerebellum and Cerebellar Disorders (Manto M, Schmahmann JD, Rossi F, Gruol DL, Koibuchi N eds), pp237–255. Dordrecht: Springer Netherlands.
Sauer B, Henderson N (1988) Site-specific DNA recombination in mammalian cells by the Cre recombinase of bacteriophage P1. Proc Natl Acad Sci U S A 85:5166–5170.
Schmidt-Supprian M, Rajewsky K (2007) Vagaries of conditional gene targeting. Nat Immunol 8:665–668.
Soda T, Mapelli L, Locatelli F, Botta L, Goldfarb M, Prestori F, D'Angelo E (2019) Hyperexcitability and hyperplasticity disrupt cerebellar signal transfer in the IB2 KO mouse model of autism. Journal of Neuroscience 39:2383–2397.
Soriano P (1999) Generalized lacZ expression with the ROSA26 Cre reporter strain. Nat Genet 21:70–71.
Stone JS, Pujol R, Nguyen TB, Cox BC (2021) The Transcription Factor Sox2 Is Required to Maintain the Cell Type-Specific Properties and Innervation of Type II Vestibular Hair Cells in Adult Mice. J Neurosci 41:6217–6233.
Tsien JZ (2016) Cre-Lox Neurogenetics: 20 Years of Versatile Applications in Brain Research and Counting…. Front Genet 7:19.
Tsien JZ, Chen DF, Gerber D, Tom C, Mercer EH, Anderson DJ, Mayford M, Kandel ER, Tonegawa S (1996) Subregion- and Cell Type–Restricted Gene Knockout in Mouse Brain. Cell 87:1317–1326.
Wang S, Liu B, Tao HW, Xia K, Zhang LI (2009) A Genetic Strategy for Stochastic Gene Activation with Regulated Sparseness (STARS). PLoS One 4:e4200.
Wang VY, Rose MF, Zoghbi HY (2005) Math1 expression redefines the rhombic lip derivatives and reveals novel lineages within the brainstem and cerebellum. Neuron 48:31–43.
Wang X, McCoy PA, Rodriguiz RM, Pan Y, Je HS, Roberts AC, Kim CJ, Berrios J, Colvin JS, Bousquet-Moore D, Lorenzo I, Wu G, Weinberg RJ, Ehlers MD, Philpot BD, Beaudet AL, Wetsel WC, Jiang YH (2011) Synaptic dysfunction and abnormal behaviors in mice lacking major isoforms of Shank3. Human Molecular Genetics 20:3093–3108.
Wang X, Xu Q, Bey AL, Lee Y, Jiang YH (2014) Transcriptional and functional complexity of Shank3 provides a molecular framework to understand the phenotypic heterogeneity of SHANK3 causing autism and Shank3 mutant mice. Molecular Autism 5:30.

549 Wang XT, Zhou L, Cai XY, Xu FX, Xu ZH, Li XY, Shen Y (2021) Deletion of Mea6 in Cerebellar Granule
550 Cells Impairs Synaptic Development and Motor Performance. Frontiers in Cell and
551 Developmental Biology 8:1850.
552 Wijayatunge R, Liu F, Shpargel KB, Wayne NJ, Chan U, Boua J-V, Magnuson T, West AE (2018) The
553 histone demethylase Kdm6b regulates a mature gene expression program in differentiating
554 cerebellar granule neurons. Mol Cell Neurosci 87:4–17.
555 Wu S-R, Butts JC, Caudill MS, Revelli J-P, Dhindsa RS, Durham MA, Zoghbi HY (2023) Atoh1 drives
556 the heterogeneity of the pontine nuclei neurons and promotes their differentiation. Sci Adv
557 9:eadg1671.
558 Zhang R, Huang D, Gasparini S, Geerling JC (2024) Efferent projections of Nps-expressing neurons in
559 the parabrachial region. J Comp Neurol 532:e25629.
560 Zheng B, Sage M, Sheppeard EA, Jurecic V, Bradley A (2000) Engineering Mouse Chromosomes with
561 Cre-loxP: Range, Efficiency, and Somatic Applications. Mol Cell Biol 20:648–655.
562

563

564 **Figure 1**



565

Fig. 1: *Atoh1-CreER^{TM+};Ai14^{+}* mice exhibit tdTomato expression specifically in the cerebellum. **(A)** Schematic of the breeding strategy used to generate *Atoh1-CreER^{TM+};Ai14^{+}* and *Atoh1-CreER^{TM-};Ai14^{+}* (control) mice. **(B-E)** Representative sagittal brain sections from *Atoh1-CreER^{TM+};Ai14^{+}* mice showing tdTomato fluorescence (magenta) **(B)**, NeuN immunostaining (yellow) **(C)**, Hoechst nuclear staining (cyan) **(D)**, and the merged image **(E)**. **(B'-E')** Higher magnification images corresponding to panels B-E, respectively. **(F-I)** Representative sagittal brain slice images from *Atoh1-CreER^{TM-};Ai14^{+}* (control) mice showing the absence of tdTomato fluorescence **(F)**, NeuN immunostaining **(G)**, Hoechst nuclear staining **(H)**, and the merged image **(I)**. **(J)** Comparison of manual versus automated quantification across 33 images (40X magnification) acquired from cerebellar lobules 2-10 from four *Atoh1-CreER^{TM+};Ai14^{+}* mouse (one sagittal brain section per mouse). **(K)** Percentage of tdTomato^{+} CGCs within each cerebellar lobule (2-10). Individual data points are shown as solid circles, and bars represent the mean ± SEM. **(L)** Pie chart showing the overall average percentage of tdTomato^{+}/NeuN^{+} (Magenta) and tdTomato^{-}/NeuN^{+} (Gray) CGCs in the cerebellum of *Atoh1-CreER^{TM+};Ai14^{+}* mice. Control: N = 3 mice; *Atoh1-CreER^{TM+};Ai14^{+}*: N = 3 mice. Two brain slices were analyzed from each *Atoh1-CreER^{TM+};Ai14^{+}* mouse, and the mean percentage of tdTomato^{+} CGCs in each lobe per mouse was used for panel K. Scale bars: B-E and F-I, 1 mm; B'-E', 20 μm. Panel A was created with BioRender.com.

584 **Figure 2**

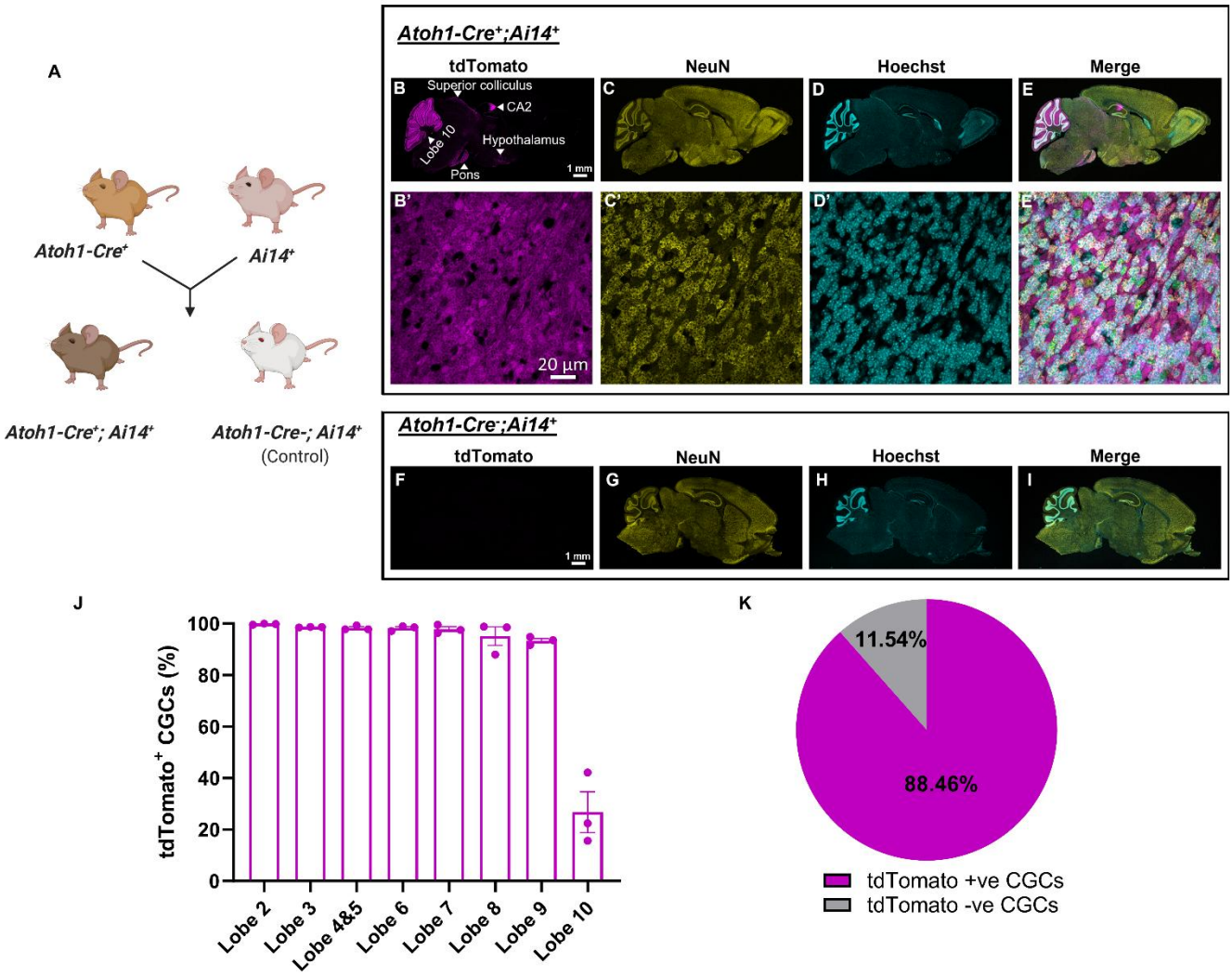

A
Atoh1-Cre+
Ai14+
Atoh1-Cre+; Ai14+
Atoh1-Cre-; Ai14+
(Control)
Atoh1-Cre+;Ai14+
tdTomato
NeuN
Hoechst
Merge
Superior colliculus
CA2
Lobe 10
Hypothalamus
Pons
1 mm
20 µm
Atoh1-Cre-;Ai14+
J
tdTomato+ CGCs (%)
100
80
60
40
20
0
Lobe 2
Lobe 3
Lobe 4&5
Lobe 6
Lobe 7
Lobe 8
Lobe 9
Lobe 10
K
11.54%
88.46%
tdTomato +ve CGCs
tdTomato -ve CGCs

Fig. 2: *Atoh1-Cre*$^{+}$*;Ai14*$^{+}$ mice show tdTomato expression in the cerebellum, with some nonspecific expression observed in other brain regions. (A) Schematic of the breeding strategy used to generate *Atoh1-Cre*$^{+}$*;Ai14*$^{+}$ and *Atoh1-Cre*$^{-}$*;Ai14*$^{+}$ (control) mice. **(B-E)** Representative sagittal brain sections from *Atoh1-Cre*$^{+}$*;Ai14*$^{+}$ mice showing tdTomato fluorescence (magenta) in the cerebellum as well as in other brain regions, including superior colliculus, hippocampus, hypothalamus, and pons **(B)**, NeuN immunostaining (yellow) **(C)**, Hoechst nuclear staining (cyan) **(D)**, and the merged image **(E)**. **(B'-E')** Higher magnification images corresponding to panels B-E, respectively. **(F-I)** Representative sagittal brain slice images from *Atoh1-Cre*$^{-}$*;Ai14*$^{+}$ (control) mice showing the absence of tdTomato fluorescence **(F)**, NeuN immunostaining **(G)**, Hoechst nuclear staining **(H)**, and the merged image **(I)**. **(J)** Percentage of tdTomato^{+} CGCs within each cerebellar lobe (lobes 2-10). Individual data points are shown as solid circles, and bars represent the mean ± SEM. **(K)** Pie chart showing the overall average percentage of tdTomato^{+}/NeuN^{+} (Magenta) and tdTomato^{-}/NeuN^{+} (Gray) CGCs in the cerebellum of *Atoh1-Cre*$^{+}$*;Ai14*$^{+}$ mice. Control: N = 3 mice; *Atoh1-Cre*$^{+}$*;Ai14*$^{+}$: N = 3 mice. Scale bars: B-E and F-I, 1 mm; B'-E', 20 µm. The image in panel A is created with BioRender.com.

Figure 3

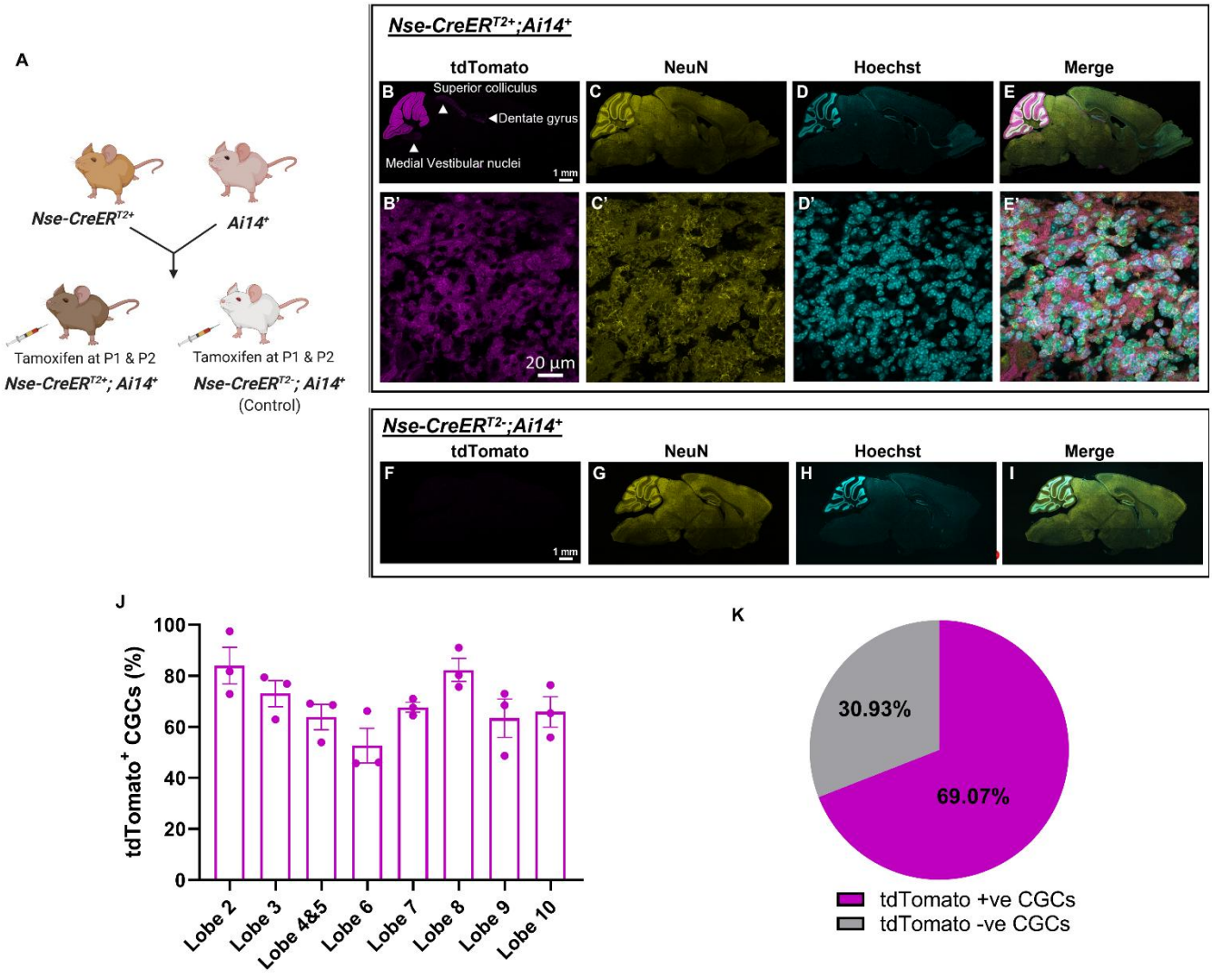

A
Nse-CreER^T2+
Ai14+
Tamoxifen at P1 & P2
Nse-CreER^T2+; Ai14+
Tamoxifen at P1 & P2
Nse-CreER^T2-; Ai14+
(Control)
Nse-CreER^T2+;Ai14+
tdTomato
NeuN
Hoechst
Merge
B
Superior colliculus
Dentate gyrus
Medial Vestibular nuclei
1 mm
C
D
E
B'
C'
D'
E'
20 µm
Nse-CreER^T2-;Ai14+
tdTomato
NeuN
Hoechst
Merge
F
G
H
I
1 mm
J
tdTomato+ CGCs (%)
100
80
60
40
20
0
Lobe 2
Lobe 3
Lobe 4&5
Lobe 6
Lobe 7
Lobe 8
Lobe 9
Lobe 10
K
30.93%
69.07%
tdTomato +ve CGCs
tdTomato -ve CGCs

Fig. 3: *Nse-CreER^{T2+};Ai14^{+}* mice show tdTomato expression in the cerebellum, with some nonspecific expression observed in other brain regions. (A) Schematic of the breeding strategy used to generate *Nse-CreER^{T2+};Ai14^{+}* and *Nse-CreER^{T2-};Ai14^{+}* (control) mice. **(B-E)** Representative sagittal brain sections from *Nse-CreER^{T2+};Ai14^{+}* mice showing tdTomato fluorescence (magenta). *Nse-CreER^{T2+};Ai14^{+}* mice showed non-specific expression of tdTomato in the superior colliculus, the hippocampus (Dentate gyrus), and the medial vestibular nuclei **(B)**, NeuN immunostaining (yellow) **(C)**, Hoechst nuclear staining (cyan) **(D)**, and the merged image **(E)**. **(B'-E')** Higher magnification images corresponding to panels B-E, respectively. **(F-I)** Representative sagittal brain slice images from *Nse-Cre^{-};Ai14^{+}* (control) mice showing the absence of tdTomato fluorescence **(F)**, NeuN immunostaining **(G)**, Hoechst nuclear staining **(H)**, and the merged image **(I)**. **(J)** Percentage of tdTomato^{+} CGCs within each cerebellar lobe (lobes 2-10). Individual data points are shown as solid circles, and bars represent the mean ± SEM. **(K)** Pie chart showing the overall average percentage of tdTomato^{+}/NeuN^{+} (Magenta) and tdTomato^{-}/NeuN^{+} (Gray) CGCs in the cerebellum of *Nse-Cre^{+};Ai14^{+}* mice. Control: N = 3 mice; *Nse-Cre^{+};Ai14^{+}*: N = 3 mice. Scale bars: B-E and F-I, 1 mm; B'-E', 20 μm. The image in panel A is created with BioRender.com.

Figure 4

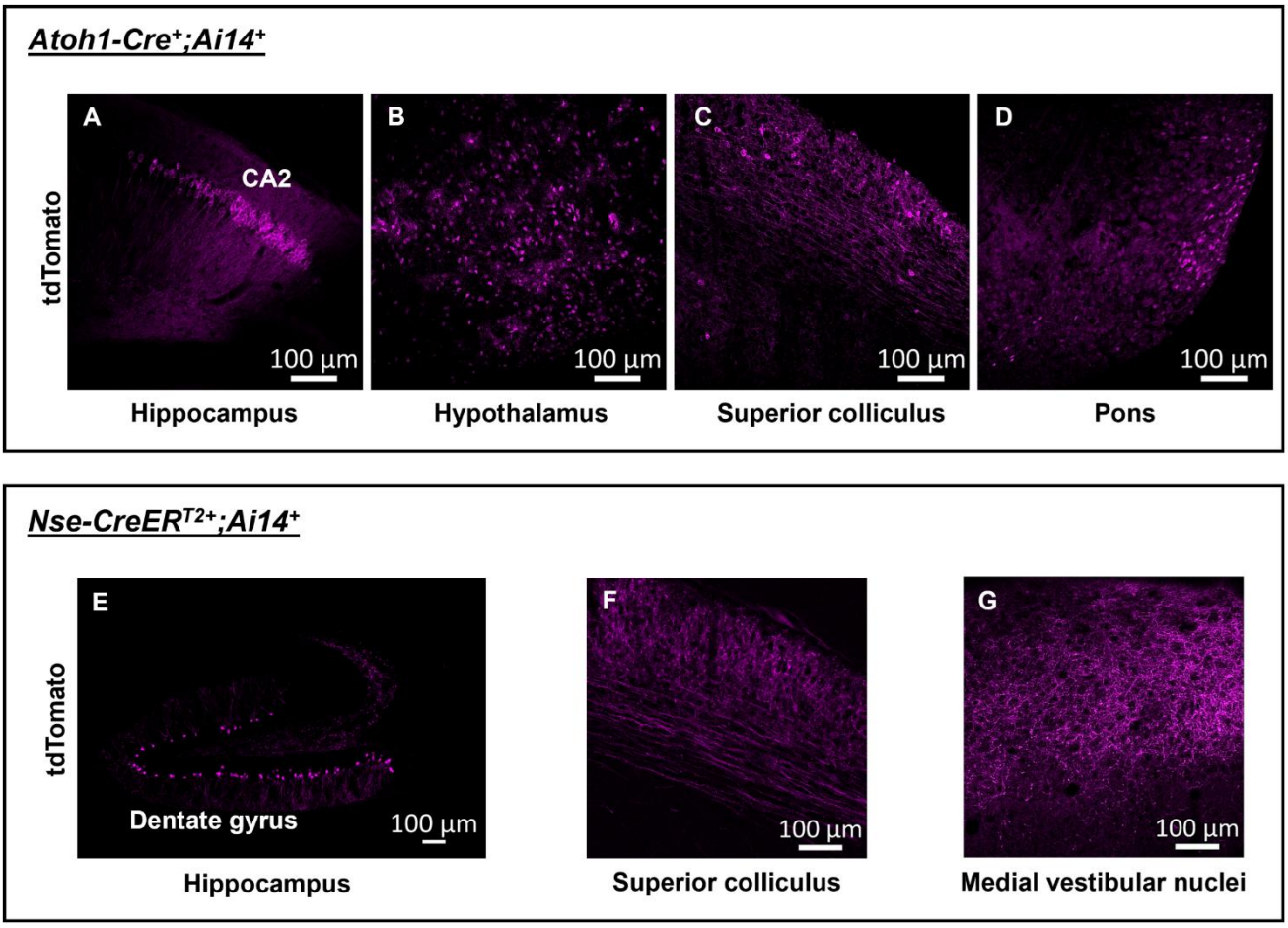
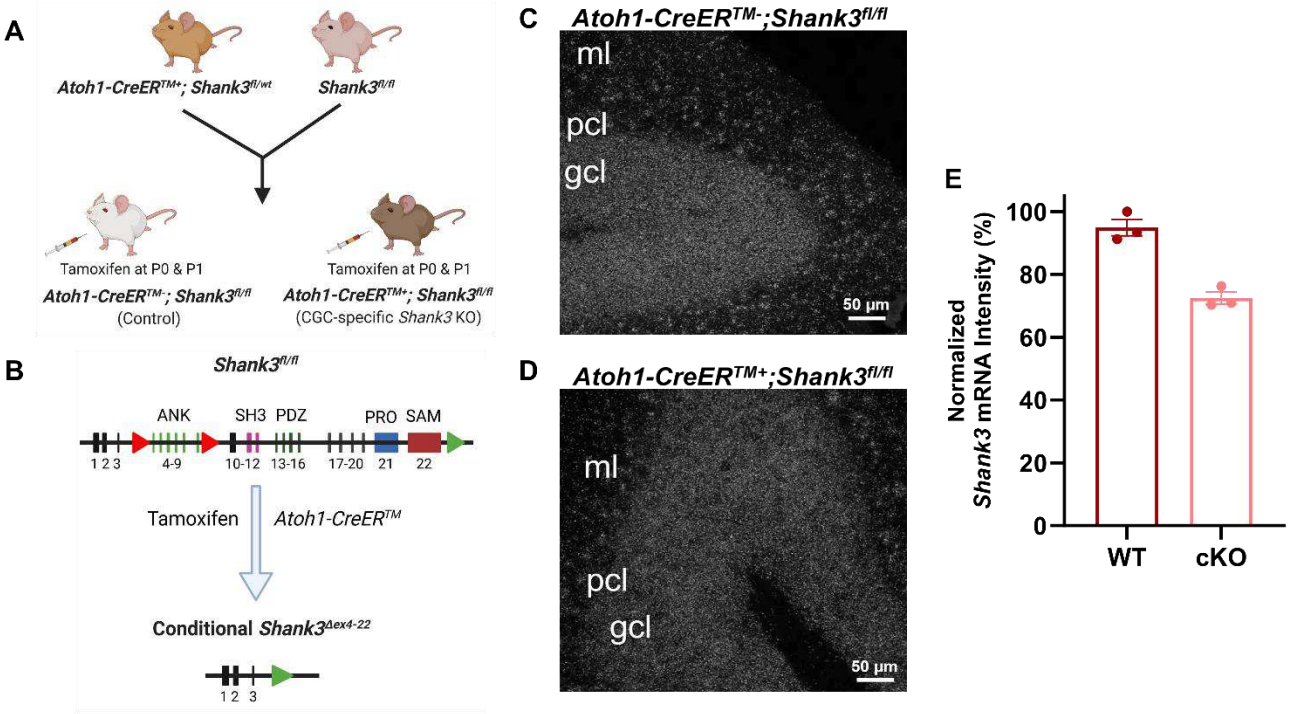

Atoh1-Cre+;Ai14+
tdTomato
A
CA2
100 µm
Hippocampus
B
100 µm
Hypothalamus
C
100 µm
Superior colliculus
D
100 µm
Pons
Nse-CreERT2+;Ai14+
tdTomato
E
Dentate gyrus
100 µm
Hippocampus
F
100 µm
Superior colliculus
G
100 µm
Medial vestibular nuclei

Fig. 4: Higher-magnification images show off-target tdTomato expression in *Atoh1-Cre*$^{+}$*;Ai14*$^{+}$ and *Nse-Cre*$^{+}$*;Ai14*$^{+}$ mice. (A-D) Representative high-magnification images showing ectopic tdTomato fluorescence (magenta) in *Atoh1-Cre*$^{+}$*;Ai14*$^{+}$ mice in the hippocampal CA2 region **(A)**, hypothalamus **(B)**, superior colliculus **(C)**, and pons **(D)**. **(E-G)** Representative high-magnification images showing ectopic tdTomato fluorescence (magenta) in *Nse-Cre*$^{+}$*;Ai14*$^{+}$ mice in the hippocampal dentate gyrus **(E)**, superior colliculus **(F)**, and medial vestibular nuclei **(G)**. Scale bars: A-G, 100 μm.

628 **Figure 5**



629

Fig. 5: Assessment of *Shank3* mRNA signal by RNAscope following *Atoh1-CreER^{TM}* induction. **(A)** Schematic of the breeding strategy used to generate *Atoh1-CreER^{TM+};Shank3$^{fl/fl}$* and *Atoh1-CreER^{TM-};Shank3$^{fl/fl}$* (control) mice. **(B)** Schematic of the generation of conditional *Shank3$^{ex\Delta 4\text{-}22}$* KO mice using a Cre-loxP strategy. *Shank3$^{fl/fl}$* mice have two loxP inserted after exon 3, 9 (red triangles), and an additional loxP at the downstream of exon 22 (green triangle). *Shank3$^{fl/fl}$* mice were crossed with *Atoh1-CreER^{TM+}* to generate conditional *Shank3$^{ex\Delta 4\text{-}22}$* KO mice. **(C, D)** Cerebellar lobes showing *Shank3* mRNA expression (in white) in *Atoh1-CreER^{TM-};Shank3$^{fl/fl}$* (control, **C**) and *Atoh1-CreER^{TM+};Shank3$^{fl/fl}$* (control) mice (cKO, **D**). **(E)** Quantification of normalized *Shank3* mRNA expression between control (red) and cKO (light red). Individual data points are shown as circles, and bars represent the mean ± SEM. Control: N = 3 mice; cKO: N = 3 mice. Abbreviations: ANK: ankyrin repeat domain, SH3: SRC homology, PDZ: PSD-95-discs large-zone occludens-1, PRO: proline-rich domain, SAM: sterile alpha motif. The image in panel B was modified from Drapeau et al., 2018. Scale bars: C-D, 50 µm.The images in panels A and B were created with BioRender.com.